Journal of Physics D:
Applied Physics

PAPER • **OPEN ACCESS**

Dominant heating mechanisms in a surface barrier discharge

To cite this article: B Gilbart *et al* 2021 *J. Phys. D: Appl. Phys.* **54** 175202

OPEN ACCESS
IOP Publishing
Journal of Physics D: Applied Physics
J. Phys. D: Appl. Phys. **54** (2021) 175202 (11pp)
https://doi.org/10.1088/1361-6463/abdff4

Dominant heating mechanisms in a surface barrier discharge

B Gilbart, A Dickenson, J L Walsh and M I Hasan

Centre for Plasma Microbiology, Department of Electrical Engineering, University of Liverpool, Brownlow Hill, L69 3GJ Liverpool, United Kingdom

E-mail: mihasan@liverpool.ac.uk

Received 10 November 2020, revised 14 January 2021
Accepted for publication 26 January 2021
Published 12 February 2021

Abstract

In computational models of atmospheric pressure surface barrier discharges (SBDs) the role of heating of the dielectric material and the quiescent gas is often neglected, impacting the accuracy of the calculated chemical kinetics. In this contribution, a two-dimensional fluid model of an SBD was developed and experimentally validated to determine the relative contribution of the dominant heat transfer mechanisms and to quantify the impact of discharge heating on the resultant chemistry. Three heating mechanisms were examined, including electron heating of the background gas due to inelastic collisions, ion bombardment of the dielectric surface and dielectric heating by the time-varying electric field. It was shown that electron heating of the background gas was not significant enough to account for the experimentally observed increase in temperature of the dielectric material, despite being the dominant heating mechanism of the gas close to the electrode. Dielectric heating was ruled out as the frequency response of typical dielectric materials used in SBD devices does not overlap with the experimentally observed power spectrum of an SBD excited at kHz frequencies. The ionic flux heating was found to be the dominant heating mechanism of the dielectric material and the downstream flow driven by the SBD. The largest impact of plasma heating on discharge chemistry was found in reactive nitrogen species (RNS) production, where the densities of RNSs increased when an appropriate treatment of heating was adopted. This had a marked effect on the discharge chemistry, with the concentration of NO_2 increasing by almost 50% compared to the idealized constant temperature case.

Supplementary material for this article is available online

Keywords: low temperature plasma, atmospheric pressure plasma, surface barrier discharge

(Some figures may appear in colour only in the online journal)

1. Introduction

The surface barrier discharge (SBD) is a simple electrode configuration that is often employed for the generation of atmospheric-pressure plasma. In an SBD a dielectric layer separates the two electrodes driving the discharge. When a suitably high potential difference is applied between the electrodes, gas breakdown occurs, generating plasma on the surface of the dielectric.

Recently, SBDs have seen increased interest, driven by the fact that when operated in air, they generate a variety of reactive species, including O_3, NO_2, O_2^+, free radicals and many other species. As many of these species are highly effective at inactivating bacteria [1–3], SBDs are suitable for a wide range of applications including the decontamination of industrial materials [4, 5], food processing equipment [6, 7], and biological tissues [8, 9]. Another advantage of SBDs which makes

them suitable for a range of applications is their scalability in comparison to many other discharge configurations [10–12]. Considering that applications vary in terms of the reactive species they require, determining the chemical processes leading to the generation of reactive species has been the focus of many studies [13–15]. Experimental techniques such as Fourier transform infrared spectroscopy and ultraviolet spectroscopy have been used to determine and quantify the generated reactive species in SBDs [16]. Despite the valuable information such techniques provide, they cannot be used to decipher all of the intricate chemical pathways leading to the formation of important chemical species; thus, numerical models often play a key role in improving our understanding of the physicochemical properties of the discharge [13, 15, 17–19].

A common simplifying assumption in many numerical models is that both the discharge and the dielectric have a constant, uniform temperature distribution throughout. Experimentally, atmospheric pressure discharges in air are known to heat up as they operate for an extended period, where they take minutes of operation until arriving to their steady-state operation temperatures. A noticeable change in the gas temperature can influence multiple aspects of the discharge. These include a change in the electron and ion transport properties; chemical reaction rates; maximum streamer velocity; sheath thickness and maximum streamer length [20]. Some reaction coefficients are highly sensitive to temperature. For example, the rate coefficient of the reaction between O_3 and NO to generate NO_2, being one of the dominant reactions for generating NO_2 [16], increases by 32% for an increase of 20 °C from room temperature. Clearly, an accumulation of such factors in large chemistry models could alter the results significantly, ultimately resulting in large errors in the predicted densities of the species involved in those reactions.

Few studies have focused on heating in SBDs. For example, Nudnova *et al* [21] reported that in an atmospheric pressure air system operating under 1000 Td, up to 54% of the discharge power goes into heating, the temperature distribution in an SBD was characterized using infrared thermography (IRT) measurements. In the work of Tirumula and colleagues [22] it was suggested that heat transfer to the downstream region is predominately through convection, but that the near electrode region may be heated by ion bombardment. Using the same technique, it was reported that surface temperature increases linearly with frequency and quadratically with voltage amplitude in an SBD [23]. IRT was also used to experimentally identify a positive correlation between the applied voltage and the dielectric surface temperature. This showed that different dielectric materials produce different thermal responses [24], which can either be due to different dielectric heating properties or different plasma properties. It has also been reported using IRT that a hotter dielectric surface produced higher flow velocities but also consumed more power [25].

Despite the wide use of IRT experimentally, its accuracy is unclear when dealing with plasmas because their emissivity is non-uniform [24]. Consequently, only measurements of the gas temperature distributions in the afterglow, i.e. after the plasma is switched off, can be accurately obtained experimentally to avoid the uncertainty in the plasma's emissivity. Gas or surface temperatures outside the discharge region could also be measured during discharge operation. Considering that most of the chemical processes occur in the discharge region during operation, it is vital to obtain accurate temperature distributions for this region during the operation of the discharge. In this work, an experimentally validated model of an SBD is developed and used to compute the temperature as function of space and time of a typical SBD, in addition to identifying the dominant heating mechanisms.

Considering that SBD discharges consist of many streamers with a high-power density yet typically short duration of tens of nanoseconds [26], it is possible to identify the potential routes of heat transfer in a typical SBD. When the plasma is first ignited in air it is known to heat the gas at the point of ignition [27], primarily through electron–gas molecule collisions, which can lead to convective heat transfer to the dielectric surface. This mechanism is referred to as electron heating. Secondly, when streamers propagate on the dielectric surface, ions from the streamer heads bombard the dielectric surface with relatively high energy that may extend up to hundreds of eV [28]. The kinetic energy of the ions then dissipates into the dielectric as heat, causing the dielectric temperature to rise and thus causing a convective heat transfer from the dielectric to the gas. This is referred to as ion-flux heating. A third potential mechanism is dielectric heating. This occurs due to a time-varying electric field in the GHz frequency range, where a peak exists in the imaginary component of the permittivity for most dielectric materials [29]. Physically this means that the dielectric molecules align themselves with the electric field lines. As the field is constantly oscillating, the molecules continually rotate to re-align, dissipating their kinetic energy into heat, causing the dielectric temperature to rise. This causes convective heat transfer from the dielectric to the gas.

2. Methods

A two-dimensional (2D) plasma fluid model was developed based on our previous work [16], describing the plasma dynamics and the resulting flow and heating of the background gas and dielectric. Then the chemical model from [16] is used to evaluate the impact of heating on the discharge chemistry. The geometry describes that of an experimental setup shown in figure 1, which was used to validate the model by comparing the measured dielectric temperature to that predicted by the model under identical operational parameters.

2.1. Experimental setup

To validate the model, an experiment was set up to measure the average temperature increase in the dielectric of an SBD. The dielectric was a 2 mm thick slab made from alumina (Al_2O_3), while aluminum (Al) was used to form the four fingered shape powered electrode around which the discharge formed, as seen operating in figure 1(d). The powered electrode measured 35 mm across and 35 mm long, with four fingers with widths of 5 mm and lengths of 30 mm, each separated by a 5 mm gap. The ground electrode was formed by a planar aluminum

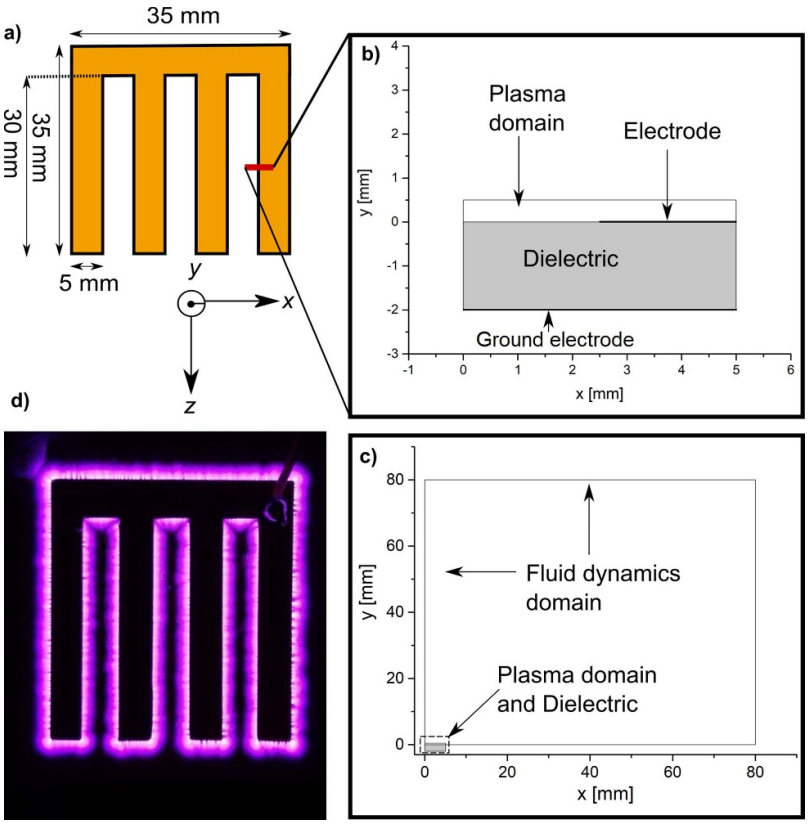

Figure 1. (a) Schematic of the electrode geometry; (b) close-up of the computational domain of the model; (c) complete computational domain; (d) an image of the electrode during discharge operation.

sheet measuring 40 × 40 mm^2 adhered to the opposing side of the dielectric. A K-type thermocouple was attached to the alumina surface near the powered electrode using thermally conductive epoxy and was used to measure the temperature of the dielectric during discharge operation. The thermocouple was attached to the dielectric at one of its corners. The point of attachment made no difference to the measured temperature.

The experiment was carried out at atmospheric pressure with the ambient environment being at a typical room temperature of 299 K. The setup was not insulated in any way, so heat could be freely convected away from the SBD. A home-made power source was used to apply a 25 kHz sinusoidal voltage, with a variable voltage to the powered electrode. Current and voltage waveforms were recorded on a Tektronix DPO 5054 digital oscilloscope using a Pearson 115 617 current probe and a Tektronix P6015A voltage probe. The discharge power was calculated by oscilloscope by multiplying the current and the voltage waveforms and averaging the product over multiple periods. Temperature measurements were taken every 10 s for the first minute of operation, then every 60 s after that for discharge powers of 5, 10 and 15 W.

2.2. Numerical model

The numerical model consisted of two parts: a plasma model and a fluid dynamics model. The plasma model is the most computationally intensive, hence it was only solved over a period of one applied voltage waveform and only in the spatial domain immediately above the electrode, as shown in figure 1(b). The computational domain represents a vertical cross-section of the discharge configuration, which assumes the discharge configuration is symmetrical around the domain, i.e. mirrored at $x = 0$. The plasma model consisted of the mass continuity equation (1), which was solved for all species included in the model, and the electron energy density equation (3) [30]:

$$\frac{\partial n_k}{\partial t} + \nabla \cdot \left(\vec{\Gamma}_k\right) = R_k; \tag{1}$$

$$\vec{\Gamma_k} = -\mu_k n_k \vec{E} - D_k \nabla n_k; \tag{2}$$

$$\frac{\partial n_\varepsilon}{\partial t} + \nabla \cdot \left(-\mu_\varepsilon n_\varepsilon \vec{E} - D_\varepsilon \nabla n_\varepsilon\right) = S_\mathrm{e} - \vec{E} \cdot \vec{\Gamma_\mathrm{e}} \tag{3}$$

where n_k is the number density of the kth species (m^{-3}); t is time (s); $\vec{\Gamma}_k$ is the flux of the kth species (m^{-2} s^{-1}). The index k runs over six species which are e^-, O_2, O_2^+, O_2^-, N_2, N_2^+. The plasma model also accounted for 13 common reactions among these species, listed in the supplementary material (available online at stacks.iop.org/JPD/54/175202/mmedia) and are represented in equation (1) by the term R_k, which is the rate expression of the kth species (m^{-3} s^{-1}). Equation (2) explains the flux term where $\vec{E}$ is the electric field (V m^{-1}); μ_k is the mobility (m^2 V^{-1} s^{-1}) of the kth species, where it is 0 for

neutral species and D_k is the diffusion coefficient of the kth species (m^2 s^{-1}). In equation (3), n_ε is the electron energy density (eV m^{-3}), S_e is the electron collisional energy loss (eV m^{-3} s^{-1}); $\vec{\Gamma}_e$ is the electron flux (m^{-2} s^{-1}). To solve these equations, the mobility and diffusion coefficient of all six species must be found. For all species but electrons, the diffusion coefficient was taken from [13] while the mobility was calculated using the Einstein relation [31]. For electrons, the transport parameters of the electron density and the energy density were calculated from LXcat [32] data using BOLSIG+ [33], which provided the transport coefficients as functions of the electron temperature. In addition to equations (1) and (3), the plasma model solves the Poisson equation in the plasma domain and in the dielectric, which is given by equation (4):

$$-\nabla\cdot(\varepsilon_r\nabla V)=\frac{\rho_v}{\varepsilon_0}. \tag{4}$$

In equation (4), V is the electric potential (V), which is used to determine the electric field using $\vec{E}=-\nabla V$, ε_r is the relative permittivity of the media, which was set to 1 for air and 9.8 for alumina [34], ε_0 is the free space permittivity (F m^{-1}), and ρ_v is the charge density (C m^{-3}). Finally, the plasma model solves for the surface charge density ρ_s on the surface of the dielectric, which is computed by equation (5):

$$\frac{\partial\rho_s}{\partial t}=q_e\hat{n}\cdot\left(\overrightarrow{\Gamma_{N_2^+}}+\overrightarrow{\Gamma_{O_2^+}}+\overrightarrow{\Gamma_{O_2^-}}+\vec{\Gamma}_e\right) \tag{5}$$

where q_e is the charge of an electron (C), $\hat{n}$ is the normal vector to the dielectric surface and Γ represents the flux of the denoted species. This calculation assumes that the charges of all particles incident to the surface are ±1 and no reflection occurs. The fluxes are computed in equation (1).

While the plasma model is solved, three variables are evaluated at each time step and integrated in time. These are the instantaneous electro-hydro-dynamic (EHD) forces, given by equation (6) and inelastic losses by electrons due to rotational and vibrational excitations, given by equation (7). It is assumed that all inelastic energy losses by electrons are converted into heat dissipated to the background gas. The third variable is the ionic energy flux to the surface, given by equation (8), which represents the heat flux to the surface due to ion bombardment. These time-integrated variables are divided by the period, thus giving the time-averaged variables used as inputs to the fluid dynamics model.

$$F_{EHD}=\rho_v\vec{E}. \tag{6}$$

$$S_{e,inelastic}=\sum\nolimits_j\epsilon_j k_j n_e n_{N_2}+\sum\nolimits_k\epsilon_k k_k n_e n_{O_2}\,. \tag{7}$$

$$\Gamma_{heat}=\hat{n}\cdot\left(E_{N_2^+}\overrightarrow{\Gamma_{N_2^+}}+E_{O_2^+}\overrightarrow{\Gamma_{O_2^+}}+E_{O_2^-}+\overrightarrow{\Gamma_{O_2^-}}\right). \tag{8}$$

In equation (7), $\in_j$ is the energy cost per excitation (eV) and k_j is the rate coefficient of the jth reaction (m^3 s). The first summation is for excitation of nitrogen while the second is for the excitation of oxygen. In equation (8), Γ_{heat} is the heat flux term to the surface (W m^{-2}), and $E_{N_2^+}$ to $E_{O_2^-}$ are the kinetic energies of the ions as they arrive at the surface (J).

The fluid dynamics model solves for the velocity field of the mixture and the temperature everywhere in the computational domain. Consequently, the heat equation is solved in the gas and the dielectric. Its computational domain is shown in figure 1(c), which extends beyond that of the plasma model, and is solved for 60 s, which is enough to obtain a clear picture of the heating without a need to update the plasma model. This is justified by experimental observations that the applied discharge power remains relatively constant over tens of seconds of operation. The fluid dynamics model consists of the continuity equation of the mixture (1); the heat equation (9) and the Navier–Stokes equation (10).

$$mnC_p\frac{\partial T}{\partial t}=-k\nabla\cdot T+S_{e,inelastic}. \tag{9}$$

$$\rho\frac{\partial\vec{u}}{\partial t}+\rho\vec{u}\cdot\nabla\vec{u}=-\nabla P+\varsigma\nabla^2\vec{u}+F_{EHD}. \tag{10}$$

where P is the pressure (Pa); ς is the viscosity of air (Pa s) and F_{EHD} is the time-averaged electrohydrodynamic force (N m^{-3}). The initial temperature of the model is set to match that in experiment at time 0.

It should be noted that because the model is not bi-directionally coupled, meaning that the output of the fluid dynamic model does not feed into the input of the plasma model, the validity of the model is restricted to short run times, where the rise in temperature does not significantly affect the plasma's physical parameters. Therefore, the investigation presented in this work is restricted to 60 s only.

To evaluate the impact of the temperature on the chemistry, the chemical model, described fully in our previous works [16] and briefly in the supplementary material, is used in conjunction with the fluid dynamics model described here. Initially, the temperature and the flow are calculated in the fluid dynamics model and are used as inputs to the chemical model. It should be noted that the chemistry model includes more species than the list of species given in the plasma model earlier.

Typically, plasma created on the surface of an SBD consists of streamers which are thin plasma filaments, with typical widths of 10–100 μm, that propagate at typical speeds of 10^6 m s^{-1} above the dielectric surface. They have a high current density and a short lifetime of a few to tens of nanoseconds [27]. Figure 2(a) shows the instantaneous power in two cycles of the discharge, where every point is an average of 100 cycles, processed and calculated using MATLAB [35]. The power spikes both in the positive and negative half-cycle, which are clearly visible in figure 2(b), are attributed to streamers forming in the discharge.

As figure 2(c) shows, there are multiple localized streamers on the dielectric surface at a given time. This poses a challenge to any 2D model because it does not allow multiple streamers to ignite and propagate independently from one another. Consequently, applying a sinusoidal waveform in the model, despite being more consistent with experiments, will inevitably lead to a nonphysical interaction between the streamers

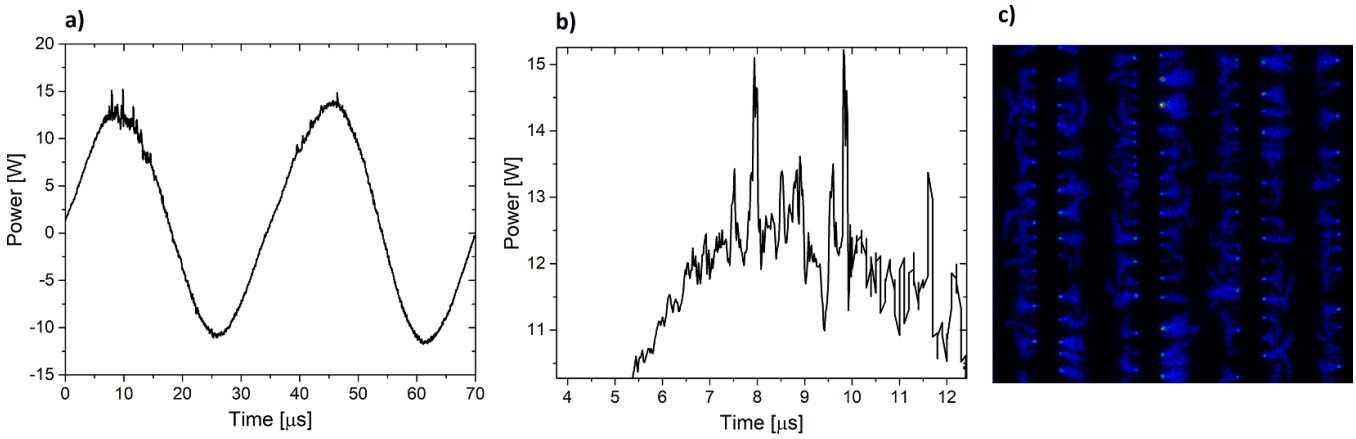

Figure 2. (a) Plot of the instantaneous power over two periods; (b) a zoomed-in view of the instantaneous power in the positive cycle; (c) ICCD images showing the streamers on the SBD. The panels shown in this figure are all for the 5 W case.

as they are forced into forming at the same position. To address this problem, an effective waveform was conceived and implemented to facilitate a direct comparison with the experimentally applied sinusoidal waveform. Both waveforms lead to the same time-averaged plasma power. It should be noted that this approach provides a compromise by partially capturing the filamentary nature of the discharge without the computational complexity of 3D models required to fully resolve the filaments. The used approach does not capture the independent nature of the different filaments igniting at different positions and different times on the electrode. Further information on the effective waveform can be found in the supplementary material.

To analyze the influence of the non-physical interaction between streamers as a result of using a 2D model to describe a 3D phenomenon, the model was run with two different waveforms. The first was a sinusoidal waveform with parameters matching those in the experimental setup. The second was an 'effective' pulsed waveform that is representative of a single streamer, where the rising and the falling edges of the pulse represent streamers in the positive half-cycle and the negative half-cycle of the sinusoidal applied waveform, respectively. The rise and fall times of the effective waveform were chosen such that the power deposited in the model agrees with that reported in the experimental setup.

The model was solved using the two waveforms for a plasma power of 10 W. All the geometric parameters and the material properties used in the model were set to match the experimental setup. The powers calculated by the model deviated by less than 10% from the corresponding experimental powers.

3. Results and discussion

3.1. Sinusoidal versus effective excitation of the model

Despite the two waveforms resulting in a similar deposited power in the model, the plasma parameters were found to be very different. Figure 3 shows the logarithms of the electron density at the time where the peak instantaneous power is reached for figure 3(a) the sinusoidal case and figure 3(b) the effective pulsed case. It is clear from a comparison of the peak electron densities that the effective pulsed waveform yields an electron density two orders of magnitude higher than that achieved with the sinusoidal waveform. Notably, the densities calculated for the pulsed case are closer to those reported for streamers in an air plasma [36–38], compared to those calculated for the sinusoidal case.

The changes in the discharge produced by the two waveforms can be explained by figure 3(c), which shows the instantaneous power density for both waveforms. The sinusoidal waveform has a lower instantaneous power density over a long period. On the other hand, the effective pulsed waveform has a higher instantaneous power density over a short period. Having a higher power density leads to having a high electron density. It should be noted here that figure 3(c) shows the calculated dissipated power; this is not the same as the experimentally measured instantaneous power, shown in figure 2, which includes a reactive contribution that cannot be removed.

Figure 3(c) also shows that the instantaneous power in the sinusoidal case, despite being driven by a waveform that matches experiments, shows significant deviation from the spikes shown in figure 2. While the instantaneous power in the effective waveform closely resembles the high-amplitude, short-duration spike observed in the measured experimental data shown in figure 2(b). This implies that the most suitable description of an SBD discharge is determined by whether the phenomena of interest stems from the filamentary nature of the discharge or the average behavior of all filaments. For example, studies of EHD force-induced flow in sinusoidal SBDs have shown to be captured correctly by models with sinusoidal excitation [39].

3.2. Model validation

Whether or not heat transfer in an SBD discharge is driven by the filamentary nature of the discharge can be inferred by solving the heat equation for both waveforms. Experimental validation of the model, in addition to providing information on the quantitative agreement between the model and

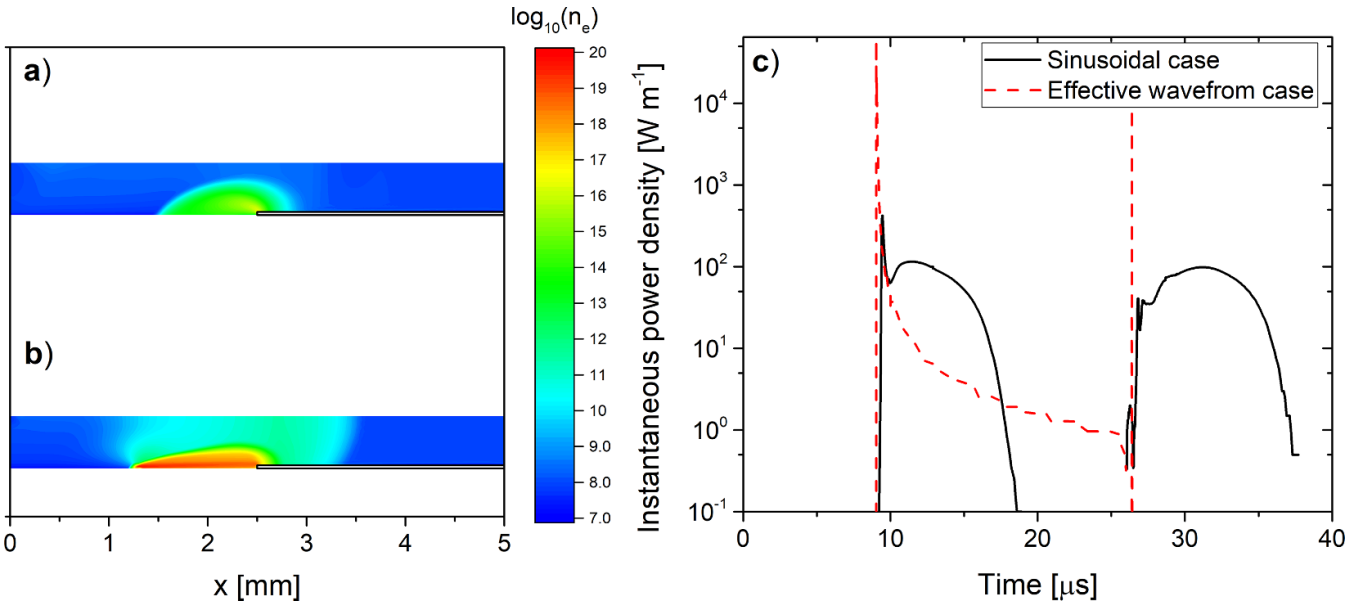

Figure 3. The logarithm of the electron density when the instantaneous power is at maximum assuming (a) sinusoidal waveform; (b) effective waveform; (c) a comparison of the instantaneous power density at the electrode between the sinusoidal case and the effective pulsed case. The curve seems discontinuous as the values drop below 0.1, which was chosen as the lower limit to highlight the details of the plotted curve. The instantaneous power at a given time is defined as the product of the voltage at the electrode at that time, multiplied by the surface integral of all charged species fluxes to the electrode at that time, which gives the current and consequently the power at that time.

the experimental setup, also enables identification of the most suitable description to follow when modelling heat transfer in SBDs. The time-averaged heat flux to the dielectric surface by both excitations is shown in figure 4(a), where it can be observed that the time-averaged heat flux in the effective excitation case is three orders of magnitude higher than that of the sinusoidal excitation case. This is a direct consequence of the difference in the plasma conditions as discussed in section 3.1.

Figure 4(b) shows a comparison between the measured average temperature of the dielectric and those computed by the model for two different powers and the two assumed excitations. The effective excitation is more consistent with experimental data. This indicates that the heat transfer processes in SBD discharges are dependent on its filamentary nature. In the rest of this work, the predictions of the model refer exclusively to the effective excitation case.

Comparing the model's results to experimental measurements, figure 4(b), shows there is a close agreement between them, with better consistency in the 10 W case. At an operating power of 5 W, the model underestimates the dielectric temperature. Critically, under such conditions the discharge appeared spatially uniform to the naked eye; however, at such low operating powers, previous intensified charged couple device (ICCD) imaging has shown that the discharge is likely to be non-uniform across the powered electrode, which will undoubtedly affect the dielectric heating within the experiment and thus explain the discrepancy with the model result.

Figure 4(b) also shows that at approximately 60 s, the temperature increases slowly in comparison to the first 10 s. This occurs as the dielectric gets closer to thermal equilibrium with its surroundings.

3.3. Dominant heating mechanisms

There are many possible mechanisms by which the plasma can heat the electrode and the background gas. In formulating the model, inelastic electron heating and ion flux heating were considered. The third mechanism, namely dielectric heating, was ruled out as the imaginary permittivity of alumina is very low in the range of frequencies observed in SBDs (0–100 MHz) [40].

Electron heating of the background gas is one possible mechanism that occurs due to inelastic collisions between the electrons and N_2 and O_2 molecules, which leads to vibrational and rotational excitation of these molecules. It is assumed that all the electron energy lost in rotational and vibrational excitations ultimately results in a rise of transitional temperature in the background gas. This assumption is based on the fast quenching of vibrationally excited states at atmospheric pressure, which limits the number of molecules reaching the higher vibrational levels necessary for chemical reactions, which is applicable even at pressures as low as 100 Torr [41]. The second possible heating mechanism is the ionic flux to the dielectric surface. The propagation of a streamer is driven by the strong electric field at its head. When the streamer head propagates on a surface, as is the case in an SBD, the streamer head accelerates the ions and drives them to bombard the dielectric surface. To convert that energy into a heat flux, it is assumed that all of the kinetic energy the ions have as they bombard the surface is dissipated as heat. This is justified by the experimental evidence that air plasmas in contact with an alumina surface show no evidence of sputtering despite extended periods of operation time [42]. Thus, both mechanisms were deemed unlikely to be significant. Data on energy

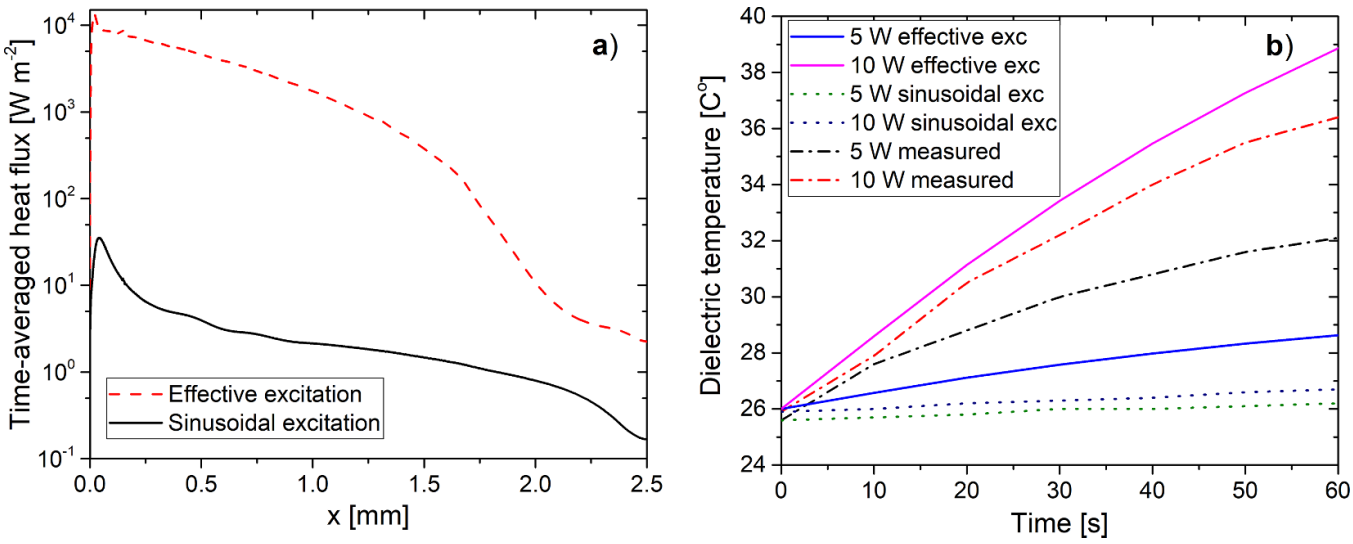

Figure 4. (a) The time-averaged heat fluxes to the dielectric surface for the sinusoidal and the effective waveforms. (b) A comparison of the average temperature of the dielectric between measured values and those calculated by the model.

reflection coefficients are scarce. Nevertheless, most available data indicates that the energy reflection coefficient for incident ions is low for normal incidence and is further reduced as the energy of the ions increases [43].

To investigate the contribution of each mechanism individually, the model was run with only electron heating, calculated by the heat equation. Then, the results were compared to the solution that included both mechanisms. Figure 5 shows the increase in the temperature after 60 s, where figure 5(a) shows the electron heating contribution while figure 5(b) shows the total contribution of both included heating mechanisms. Focusing on figure 5(a), the strongest effect of electron heating by the plasma is observed at the tip of the electrode, where an increase of 15 °C is observed. This increase becomes significantly weaker further from the electrode, reaching almost ambient temperature approximately 1 mm downstream. This is attributed to the strong electric field at the edge of the electrode, which leads to high mean electron energy in that region. Considering that the flow velocity on the surface is zero due to friction, it becomes clear why the maximum temperature increase occurs on the surface. Moving further from the surface, convection driven by EHD forces causes gas cooling. It should be noted that EHD forces in an SBD cause the gas to flow in the direction of propagation of the streamers. In the SBD configuration considered in this investigation, the streamers from two opposite electrodes meet in the center of the gap where the discharge occurs. The flows induced by both streamers coalesce, forming a perpendicular flow to the dielectric's surface as shown at $x = 0$ in figure 5 [44].

Figure 5 also shows that there is a plume of hot gas at $x = 0$, which coincides with the perpendicular flow described earlier. Its formation can be explained by the fact that the gas feeding into the perpendicular flow passes by the electrode's edge and the dielectric surface, which due to convective cooling carries some of the heat away with it. This results in the perpendicular gas flow becoming hotter than the ambient flow, appearing as a plume at the boundary $x = 0$.

In terms of the heating of the dielectric and the subsequent induced perpendicular flow, electron heating plays a minimal role. This can be understood in terms of the difference in density between air (1.2 kg m^{-3}) and alumina (3.9×10^3 kg m^{-3}). Considering that alumina's density is three orders of magnitude higher, a very large thermal flux is required to raise its temperature, which will require a very large difference in temperature between air and alumina.

When the ionic heat flux contribution is added, as shown in figure 5(b), the temperature at the edge of the electrode increased by 5 °C in comparison to the case of electron heating only. This shows that the gas heating at the edge of the electrode is dominated by electron heating. Figure 5(b) also shows that the dielectric's temperature increased by 13 °C, indicating that the increase in the dielectric temperature is entirely due to ionic heat fluxes. The induced perpendicular flow at $x = 0$ has a temperature increase of 6 °C when the ionic flux is considered. Based on these results it can be concluded that the dominant heating mechanism of the perpendicular flow is convective heat transfer from the dielectric.

These findings have two important implications for the modelling of the chemical dynamics in an SBD. The first is related to the chemistry generated in the discharge. Considering that electron heating is dominant close to the edge of the electrode, where it has been reported that most of the chemical reactions of short-lived species occur [13], this region has the greatest impact on the discharge chemistry. As chemical reactions between the long-lived species predominantly occur in the perpendicular flow induced by the SBD [16], the dissipated power within the discharge affects the chemistry of the long-lived species indirectly through heating of the dielectric material, which in turn heats the resultant perpendicular gas flow.

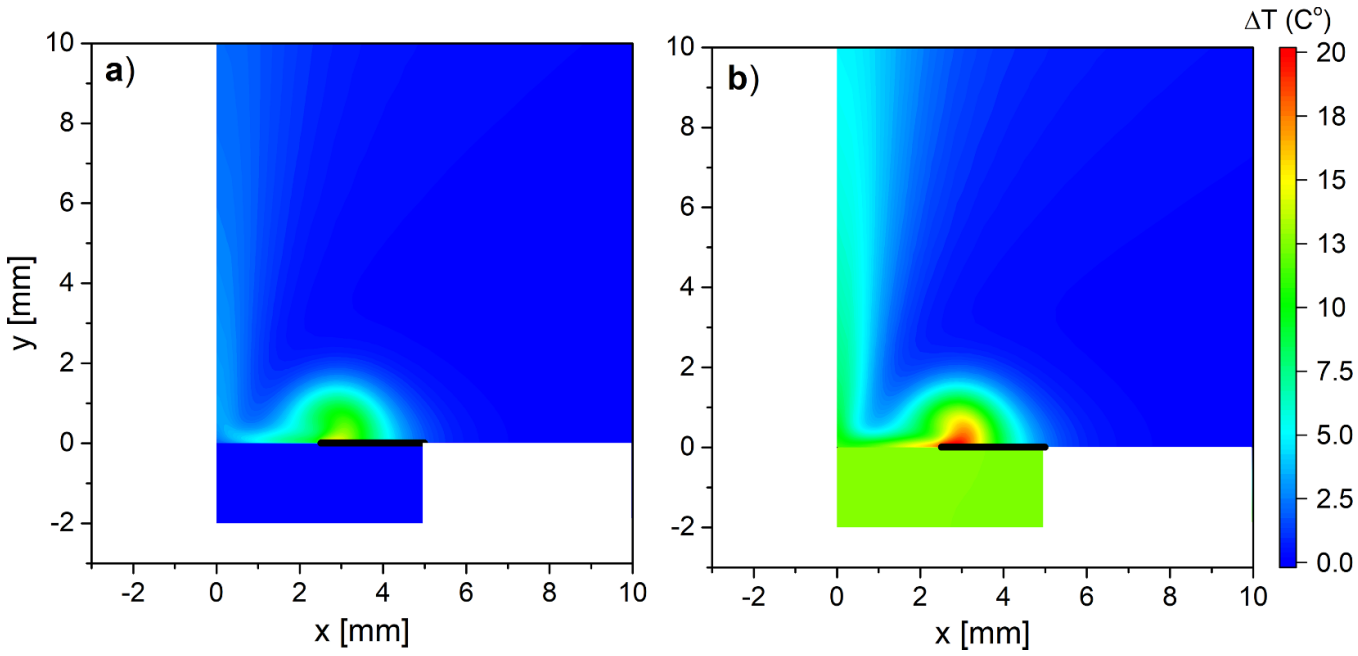

Figure 5. A 2D map of the increase in temperature after 60 s of discharge operation, calculated by the model for a power of 10 W assuming (a) electron heating only is calculated, and (b) electron heating and ionic fluxes are calculated.

Another heating mechanism that was considered but not included in the model was dielectric heating, where it is known that the imaginary part of the permittivity of most dielectrics has a peak in the GHz frequency range. This has the potential to correspond with the characteristic time of the ignition and propagation of streamers in SBD. For Al_2O_3, the dielectric response peaks at 10 GHz [40]. By performing a Fourier transform on the dissipated plasma power (data shown in supplementary material), it was found that a significant portion of the total power lies in the frequency spectrum below 60 MHz. This makes it unlikely that the power in the frequency range corresponding to the peak of the dielectric response is enough to cause any noticeable heating. In addition, the dielectric response of Al_2O_3 is known to be small [45]. Based on this analysis it is unlikely that dielectric heating would have a noticeable impact.

3.4. Impact on chemical kinetics

To quantify the significance of accounting for the described heating mechanisms when modelling SBDs, figure 6 shows the impact of each heating mechanism on the density of various reactive species. Figure 6(a) shows the 2D density of O_3 for the 10 W case with the temperature distribution computed by the model. The O_3 concentration is highest at the electrode's edge where most of the short-lived species are generated as reported in [16], and where the velocity is close to zero due to the proximity of the dielectric surface and the electrode, which results in a longer residence time and thus a higher density. Further from the electrode, gas convection transports O_3 into the perpendicular flow thus reducing its density on the dielectric surface. Figures 6(b) and (c) show the densities of O_3 and NO_2 along the symmetry axis at $x = 0$, thus showing the densities as a function of distance from the surface of the dielectric. Both O_3 and NO_2 were specifically shown in figures 6(c) and 6(d) as they show the least and the most affected species respectively when the temperature is varied. All other species vary in that range. The chemical model was solved under a constant plasma power with three test cases in terms of temperature. The first is assuming that the temperature everywhere in the domain is the room temperature (ignoring heating completely). This is the approach taken by most SBD models. The second test case assumed the temperature at any point is computed by the model, which represents the self-consistent method for modelling the chemistry (the temperature distribution is shown in figure 5(b). The third test case sets the electrode temperature at 55 °C (30 °C above room temperature), allowing the heat to be convected to the gas. The assumption of this temperature is made to provide an upper limit analysis of the influence of temperature on the chemistry. Such temperatures have been recorded after minutes of SBD operation under high power conditions [21, 23].

Comparing the densities computed for the three cases, the difference that temperature alone makes can be observed. The difference in the density of O_3 among the three test-cases is negligible. Conversely, NO_2 density shows a clear positive correlation with temperature. Therefore, a comprehensive treatment of plasma heating mechanisms noticeably increases the rate of NO_2 production due to the strong dependence of its dominant production mechanism on the temperature. In the simulated case, an increase by a factor of 20% is observed in NO_2 density along the perpendicular flow axis.

For the case where a temperature of 55 °C is assumed for the dielectric, the NO_2 density increases by a factor of 40% in comparison to that of having room temperature. Other species densities that are affected include NO, which increases by 14%

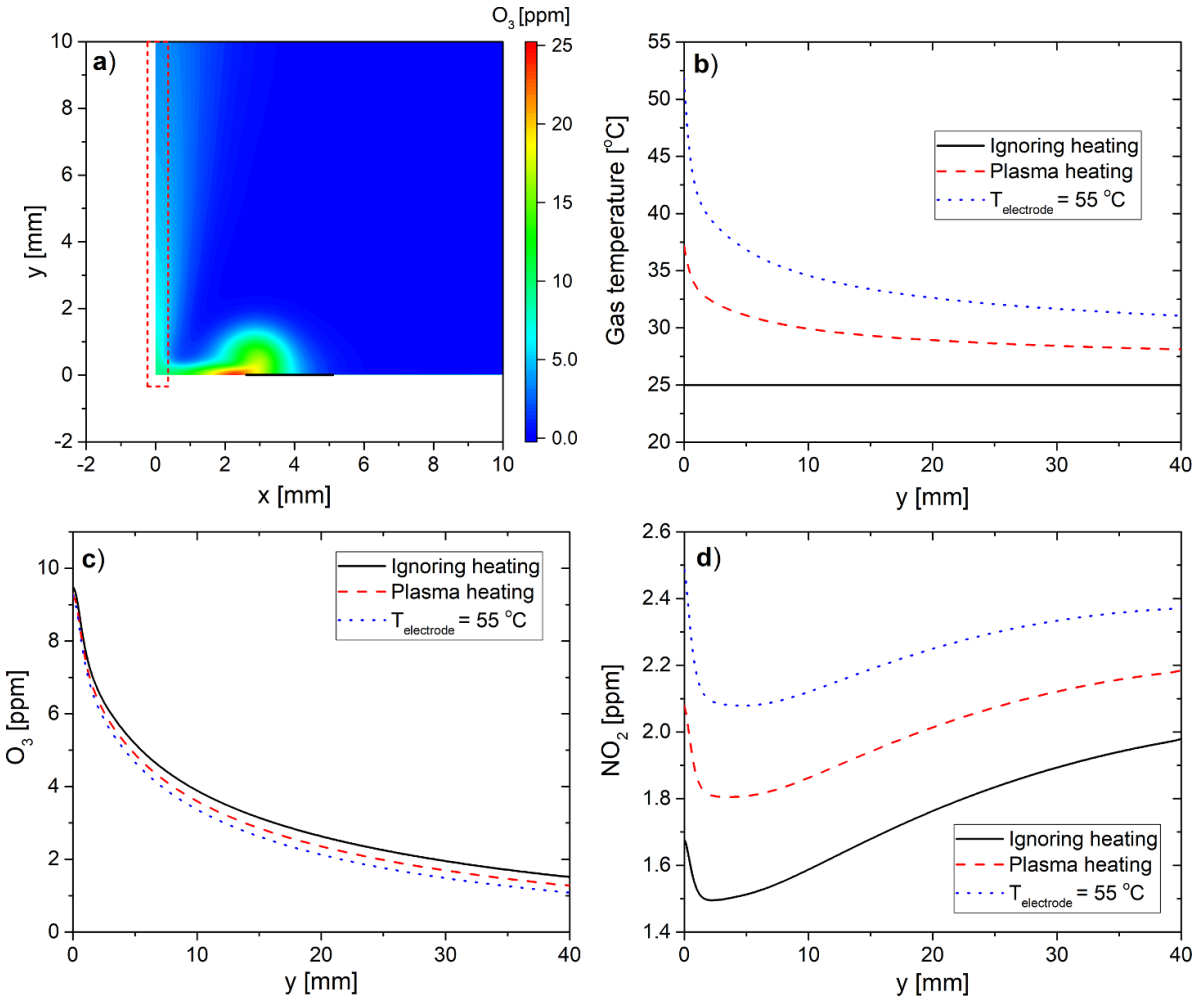

Figure 6. (a) 2D map of the O_3 density around the discharge in parts per million; (b) the temperature along the boundary shown in the red box in (a) for the three test case; (c) a cut-line of the O_3 density along the boundary shown in a red box in a) when ignoring plasma heating (black solid line), including plasma heating (red dashed line) and when only the heat from the electrode (blue dotted line); (d) a cut-line of the NO_2 density along the line shown in a red box in (a) when ignoring plasma heating (black solid line), including plasma heating (red dashed line) and when only the heat from the electrode (blue dotted line). The densities of the species were calculated over the entire computational domain but shown here close to the electrode as that is the area of interest in the domain.

for plasma heating assumption and by 27% for the constant dielectric temperature assumption. N_2O also increases by 15% under the plasma heating assumption and by 27% for the constant dielectric temperature assumption. These results indicate that taking the discharge heating into account is of vital importance for the accurate modeling of the discharge chemistry in an SBD. It should be noted here that this reported increase becomes increasingly significant when the residence time is considered. Considering that both the simulation and experiments are done assuming the discharge operates in open air, this means the residence time of the gas in the discharge region is small. In closed systems, however, the residence time is much longer and thus the difference due to plasma heating will amplify significantly over time.

4. Conclusion

In this work, a 2D experimentally validated numerical model was developed and implemented to determine the underlying mechanisms responsible for heat transfer in an SBD. It was shown that many aspects of the filamentary nature of an SBD can be captured using a 2D model through the use of an effective pulsed waveform. The results showed that heating in an SBD occurs primarily due to the filamentary nature of the plasma, rather than being a result of a spatially averaged effect across the entire discharge length. Three mechanisms of heating were considered: the electron heating of the background gas, ionic heat fluxes, and dielectric heating, where the time-dependent electric field in the streamer heads causes the dipoles in the dielectric to oscillate. The results of the model show that the increase in the dielectric temperature is almost entirely due to ionic fluxes bombarding it. It is also shown that 84% of the temperature increase in the perpendicular gas flow was a result of heat convection from the dielectric surface to the gas. Thus, the ionic flux heating is the dominant heating mechanism downstream. Electron heating of the background gas accounted for approximately 75% of the temperature increase of the background gas close to the electrode, but the increase in temperature in the dielectric and

the perpendicular flow induced by EHD forces was found to be insignificant. Dielectric heating was ruled out as a significant portion of the plasma power is in a frequency range where there is no overlap with the dielectric response of the dielectric material used.

The model was subsequently used to quantify the impact of accounting for gas heating mechanisms on the generation and loss of chemical species, where it was shown that reactive nitrogen species (RNSs) species are strongly affected while reactive oxgen species (ROSs) are not. The species which had the largest variation included NO_2 which increased by a factor of 20%–40%. Indicating that plasma heating must be considered to adequately describe the discharge chemistry.

Acknowledgments

The authors JLW and MIH would like to acknowledge the support of ESPRC Grant Numbers EP/S025790/1, EP/N021347/1, and EP/T000104/1 for their support.

ORCID iDs

J L Walsh https://orcid.org/0000-0002-6318-0892
M I Hasan https://orcid.org/0000-0001-6993-933X

References

[1] Kostov K G, Rocha V, Koga-Ito C Y, Matos B M, Algatti M A, Honda R Y, Kayama M E and Mota R P 2010 Bacterial sterilization by a dielectric barrier discharge (DBD) in air *Surf. Coat. Technol.* **204** 2954–9
[2] Choi J H, Han I, Baik H K, Lee M H, Han D-W, Park J-C, Lee I-S, Song K M and Lim Y S 2006 Analysis of sterilization effect by pulsed dielectric barrier discharge *J. Electrost.* **64** 17–22
[3] Limam S 2011 Non-thermal plasma treatment of contaminated surfaces: remote exposure to atmospheric pressure dielectric barrier discharge effluent *Adv. Mater. Res.* **324** 469–72
[4] Gerhard C and Ten Bosch L 2018 Plasma jet cleaning of optics: cleaning of silver-coated mirrors by means of atmospheric pressure plasma jets *Vakuum in Forschung Und Praxis* **30** 32–35
[5] Tsai J H 2018 DC-pulse atmospheric-pressure plasma jet and dielectric barrier discharge surface treatments on fluorine-doped tin oxide for perovskite solar cell application *J. Phys. D: Appl. Phys.* **51** 025502
[6] Gavahian M and Khaneghah. A M 2019 Cold plasma as a tool for the elimination of food contaminants: recent advances and future trends *Crit. Rev. Food Sci. Nutr.* **59** 10
[7] Kim S Y 2019 Effects of packaging parameters on the inactivation of Salmonella contaminating mixed vegetables in plastic packages using atmospheric dielectric barrier discharge cold plasma treatment *J. Food Eng.* **242** 55–67
[8] Keidar M, Yan D and Sherman J H 2019 *Cold Plasma Cancer Therapy* (San Rafael, CA: Morgan & Claypool Publishing) (https://doi.org/10.1088/2053-2571/aafb9c)
[9] Kuzminova A, Kretková T, Kylián O, Hanuš J, Khalakhan I, Prukner V, Doležalová E, Šimek M and Biederman H 2017 Etching of polymers, proteins and bacterial spores by atmospheric pressure DBD plasma in air *J. Phys. D: Appl. Phys.* **50** 135201
[10] Brandenburg R 2017 Dielectric barrier discharges: progress on plasma sources and on the understanding of regimes and single filaments *Plasma Sources Sci. Technol.* **26** 053001
[11] Moreau E, Sosa R and Artana G 2008 Electric wind produced by surface plasma actuators: a new dielectric barrier discharge based on a three-electrode geometry *J. Phys. D: Appl. Phys.* **41** 115204
[12] Kunhardt E E 2000 Generation of large-volume, atmospheric-pressure, nonequilibrium plasmas *IEEE Trans. Plasma Sci.* **28** 189–200
[13] Sakiyama Y, Graves D B, Chang H-W, Shimizu T and Morfill G E 2012 Plasma chemistry model of surface microdischarge in humid air and dynamics of reactive neutral species *J. Phys. D: Appl. Phys.* **45** 425201
[14] Kogelschatz U and Baessler P 1987 Determination of nitrous oxide and dinitrogen pentoxide concentrations in the output of air-fed ozone generators of high power density *J. Int. Ozone Assoc.* **9** 195–206
[15] Singh K P 2006 Modeling of dielectric barrier discharge plasma actuator with atmospheric air chemistry *Collection of Technical Papers—37th AIAA Plasmadynamics and Lasers Conf.* vol 2 pp 576–86
[16] Dickenson A *et al* 2018 The generation and transport of reactive nitrogen species from a low temperature atmospheric pressure air plasma source *Phys. Chem.* **20** 28499–510
[17] Hasan M I and Walsh J 2016 Numerical investigation of the spatiotemporal distribution of chemical species in an atmospheric surface barrier-discharge *J. Appl. Phys.* **119** 203302
[18] Georghiou G E 2005 Numerical modelling of atmospheric pressure gas discharges leading to plasma production *J. Phys. D: Appl. Phys.* **38** R303
[19] Hsiao R C, Sung T-L, Liu C-M, Teii S, Ono S, Teii K and Ebihara K 2015 Numerical study on heat flow during catalytic dissociation of ozone in a dielectric barrier discharge ozonizer *IEEE Trans. Plasma Sci.* **43** 665–9
[20] Zhang S, Chen Z, Zhang B and Chen Y 2019 Numerical investigation on the effects of discharge conditions on a nanosecond pulsed surface dielectric barrier discharge *J. Appl. Phys.* **125** 113301
[21] Nudnova M M, Kindysheva S V, Aleksandrov N L and Starikovskii A Y 2015 Fast gas heating in N_2/O_2 mixtures under nanosecond surface dielectric barrier discharge: the effects of gas pressure and composition *Phil. Trans. R. Soc.* A **373** 20140330
[22] Tirumula R, Benard N, Moreau E, Fenot M, Lalizel G and Dorignac E 2014 Temperature characterization of dielectric barrier discharge actuators: influence of electrical and geometric parameters *J. Phys. D: Appl. Phys.* **47** 255203
[23] Jussot R 2012 Thermal characterization of a DBD plasma actuator: dielectric temperature measurements using infrared thermography *40th Fluid Dynamics Conf. and Exhibit (Chicago, IL)* (https://doi.org/10.2514/6.2010-5102)
[24] Rodrigues F F, Pascoa J C and Trancossi M 2018 Experimental analysis of dielectric barrier discharge plasma actuators thermal characteristics under external flow influence *J. Heat Transfer.* **140** 102801
[25] Erfani R 2012 Thermal characterization of a DBD plasma actuator: dielectric temperature measurements using infrared thermography *Exp. Therm. Fluid Sci.* **42** 258–64
[26] Raizer Y P 1991 *Gas Discharge Physics* (Berlin: Springer) ch 7
[27] Zhu Y, Wu Y, Cui W, Li Y and Jia M 2013 Numerical investigation of energy transfer for fast gas heating in an atmospheric nanosecond-pulsed DBD under different negative slopes *J. Phys. D: Appl. Phys.* **46** 495205

[28] Sigmund P 1987 Mechanisms and theory of physical sputtering by particle impact *Nucl. Instrum. Methods Phys. Res.* B **27** 1–20
[29] Pryor R W 2015 Modeling dielectric heating: a first principles approach *Proc. 2015 Comsol Conf.* (Boston)
[30] Chen F 2016 *Introduction to Plasma Physics and Controlled Fusion* 3rd edn (Berlin: Springer) ch 3
[31] Mason E A and McDaniel E W 1988 *Transport Properties of Ions in Gases* 1st edn (New York: Wiley)
[32] Biagi Database The plasma data exchange project (available at: www.lxcat.net) (Accessed 15 May 2019)
[33] Hagelaar G J M and Pitchford L C 2005 Solving the Boltzmann equation to obtain electron transport coefficients and rate coefficients for fluid models *Plasma Sources Sci. Technol.* **14** 722–33
[34] Engineering ToolBox 2010 Relative permittivity—the dielectric constant (available at: www.engineeringtoolbox.com/relative-permittivity-d_1660.html) (Accessed 01 May 2019)
[35] MATLAB and Statistics Toolbox Release 2012b (Natick, MA: The MathWorks, Inc.)
[36] Soloviev V R and Krivtsov V M 2014 Mechanism of streamer stopping in a surface dielectric barrier discharge *Plasma Phys. Rep.* **40** 65–77
[37] Šimek M, Ambrico P F, Hoder T, Prukner V, Dilecce G, De Benedictis S and Babický V 2018 Nanosecond imaging and emission spectroscopy of argon streamer micro-discharge developing in coplanar surface DBD *Plasma Sources Sci. Technol.* **27** 055019
[38] Cvetanović N, Galmiz O, Synek P, Zemánek M, Brablec A and Hoder T 2018 Electron density in surface barrier discharge emerging at argon/water interface: quantification for streamers and leaders *Plasma Sources Sci. Technol.* **27** 025002
[39] Lagmich Y, Callegari T, Unfer T, Pitchford L C and Boeuf J P 2007 Electrohydrodynamic force and scaling laws in surface dielectric barrier discharge *Appl. Phys. Lett.* **90** 051502
[40] Vila R, Gonzalez M, Molla J and Ibarra A 1998 Dielectric spectroscopy of alumina ceramics over a wide frequency range *J. Nucl. Mater.* **253** 141–8
[41] Shkurenkov I, Burnette D, Lempert W R and Adamovich I V 2014 Kinetics of excited states and radicals in a nanosecond pulse discharge and afterglow in nitrogen and air *Plasma Sources Sci. Technol.* **23** 065003
[42] Kim J, Kim S-J, Lee Y-N, Kim I-T and Cho G 2018 Discharge characteristics and plasma erosion of various dielectric materials in the dielectric barrier discharges *Appl. Sci.* **8** 1294
[43] Ordonez C A and Peterkin R E Jr 1996 Numerical determination of plasma ion reflection coefficients at a sheath-surface interface *J. Nucl. Mater.* **228** 201–6
[44] Dickenson A, Morabit Y, Hasan M I and Walsh J L 2017 Directional mass transport in an atmospheric pressure surface barrier discharge *Sci. Rep.* **7** 14003
[45] Jonscher A K 1977 The 'universal' dielectric constant *Nature* **267** 673–9